JCTC Journal of Chemical Theory and Computation

Article

pubs.acs.org/JCTC

# Molecular Dynamics Simulations and Neutron Reflectivity as an Effective Approach To Characterize Biological Membranes and Related Macromolecular Assemblies

L. Darré,[†] J. Iglesias-Fernandez,[†] A. Kohlmeyer,[‡] H. Wacklin,[*,§,∥] and C. Domene[*,†,⊥]

[†]Department of Chemistry, King's College London, Britannia House, 7 Trinity Street, London SE1 1DB, United Kingdom

[‡]Institute for Computational Molecular Science (035-07), College of Science and Technology, Temple University, 1901 N. 13th Street, Philadelphia, Pennsylvania 19122, United States

[§]European Spallation Source ESS AB, P.O. Box. 176, 22100 Lund, Sweden

[∥]Physical Chemistry, Department of Chemistry, Lund University, P.O. Box 124, 22100 Lund, Sweden

[⊥]Chemistry Research Laboratory, Mansfield Road, University of Oxford, Oxford OX1 3TA, United Kingdom

**ABSTRACT:** In combination with other spectroscopy, microscopy, and scattering techniques, neutron reflectivity is a powerful tool to characterize biological systems. Specular reflection of neutrons provides structural information at the nanometer and subnanometer length scales, probing the composition and organization of layered materials. Currently, analysis of neutron reflectivity data involves several simplifying assumptions about the structure of the sample under study, affecting the extraction and interpretation of information from the experimental data. Computer simulations can be used as a source of structural and dynamic data with atomic resolution. We present a novel tool to compare the structural properties determined by neutron reflectivity experiments with those obtained from molecular simulations. This tool allows benchmarking the ability of molecular dynamics simulations to reproduce experimental data, but it also promotes unbiased interpretation of experimentally determined quantities. Two application examples are presented to illustrate the capabilities of the new tool. The first example is the generation of reflectivity profiles for a 1,2-dimyristoyl-*sn*-glycero-3-phosphocholine (DMPC) lipid bilayer from molecular dynamics simulations using data from both atomistic and coarse-grained models, and comparison with experimentally measured data. The second example is the calculation of lipid volume changes with temperature and composition from all atoms simulations of single and mixed 1,2-di-palmitoyl-*sn*-glycero-3-phosphocholine (DOPC) and 1,2-dihexadecanoyl-*sn*-glycero-3-phosphocholine (DPPC) bilayers.

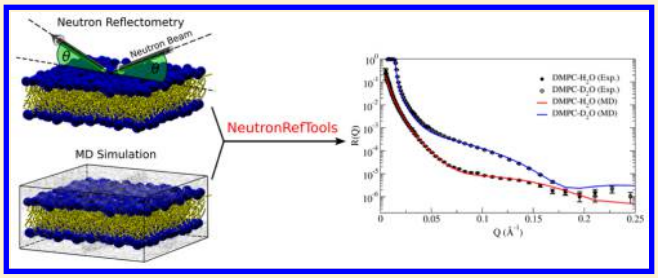


## INTRODUCTION

Surfaces, interfaces, and thin films, which are ubiquitous in nature, are planar structures that define the spatial boundary between two different media. In biological systems, boundaries between many phases are defined by soft interfaces, (i.e., membranes and biopolymers) embedded in physiological electrolyte solutions. For example, biological membranes are vital components delimiting the outer boundary of the cell from the environment, as well as that of intracellular compartments within the cytoplasm. They serve as smart filters, allowing for functional compartmentalization, protection from toxic substances, and transport of metabolites. In addition, they provide a two-dimensional physicochemical framework enhancing biochemical processes, such as diffusion-limited reactions.[1] Consequently, understanding the structure of this type of systems constitutes a cornerstone of multiple biological and technological applications. These complex systems are studied by using both integrated and reconstituted model systems that closely mimic natural membranes.

Neutron reflectometry is a powerful tool for the characterization of thin films and interfaces at the nanometer length scales[2,3] and is particularly advantageous because of its ability to detect the dimensions, chemical composition, and relative location of specific molecular species, in noncrystalline, disordered thin films. This ability relies on several factors. The first of them is the sensitivity of neutrons to the coherent nuclear scattering length, an intrinsic property of the elements, which displays a particularly large difference between hydrogen (−3.74 fm) and its heavy isotope deuterium (+6.67 fm), allowing isotopic substitution to be exploited to highlight specific parts of the system. Other beneficial factors are their nondestructive nature and their long penetration ability. In addition, light elements such as hydrogen, carbon, nitrogen, and oxygen strongly scatter neutrons, thus making neutron reflectivity suitable for biological samples.

**Received:** July 2, 2015
**Published:** September 17, 2015





DOI: 10.1021/acs.jctc.5b00635
*J. Chem. Theory Comput.* 2015, 11, 4875−4884

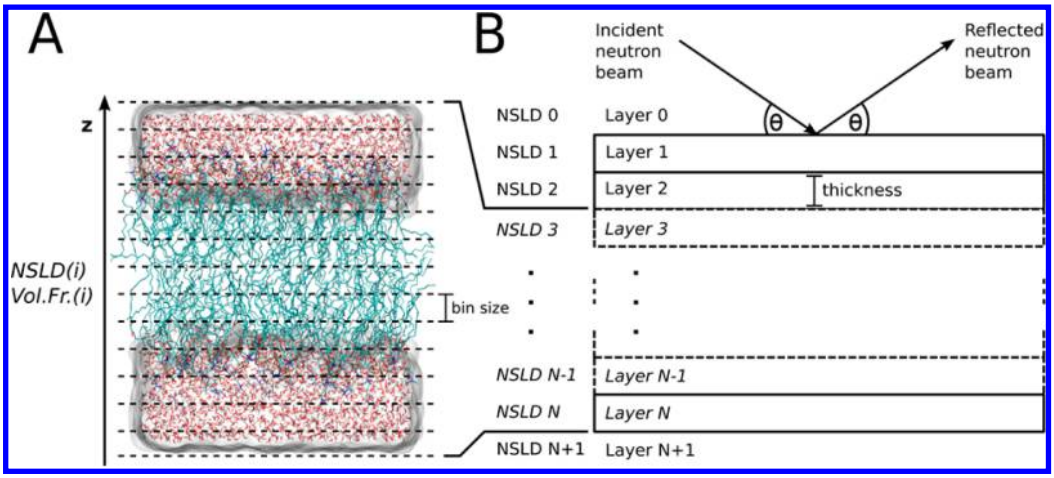


**Figure 1.** Layer model construction from MD data. (A) Model system of a 1,2-dimyristoyl-*sn*-glycero-3-phosphocholine (DMPC) bilayer/$H_2O$ shown with the membrane aligned to the $x-y$ plane. Structural information from the MD trajectory is used to build the NSLD (and/or the volume fraction) by discretizing the system in $N-2$ bins, numbered from $i = 3$ to $i = N$. (B) The discrete NSLD values from the MD trajectory are used to construct a representation of the experimental setup where layers 0, 1, 2, and $N + 1$ are used to model the environment in which the substrate is embedded. For example, in a supported DMPC bilayer system, such as the one analyzed here, layers 0 and 1 would represent silicon and silica, respectively, layer 2 could be used as an extra solvent layer to aid fitting the MD data into the experimental configuration, and layer $N + 1$ would correspond to the bulk solvent.

In a specular neutron reflection experiment, reflectivity, i.e., the ratio between the reflected and incident intensities (eq 1) of a collimated neutron beam directed at an interface at a grazing angle (Figure 1B) is measured as a function of the momentum transfer vector $Q_z$ (eq 2), which is dependent on the incident neutron beam angle ($\theta$) and wavelength ($\lambda$).

$$R = \frac{I}{I_0} \tag{1}$$

$$Q_z = \frac{4\pi \sin(\theta)}{\lambda} \tag{2}$$

The molecular organization in the direction orthogonal to the planar interface (i.e., the $z$-axis) determines the density of atoms at every value of $z$ and, since the neutron scattering length is dependent on the atomic nuclei, this defines the Neutron Scattering Length Density (NSLD) profile in that direction. The NSLD profile determines the reflectivity; thus, the latter contains the information about the molecular organization of the system. However, such information is not directly available from the reflectivity data, and typically, an initial structural guess to model the system is required. From this initial guess, the reflectivity can be calculated, using, for example, the Abeles optical matrix method[4] (see Methods), and compared to the experimentally measured data. This procedure is iterated to reach an agreement between the modeled reflectivity and the experimental reflectivity. The final outcome is a NSLD profile associated with the model generated for the molecular organization of the system. One drawback of the method is that, as in all other diffraction-based methods, phase information is lost on measuring the reflected intensity, making it difficult to determine a unique model. To overcome this limitation, multiple neutron contrasts (i.e., solute/solvent deuteration schemes) are experimentally measured and simultaneously fitted against different models. This allows incorrect models to be filtered out, often aided by additional constraints such as molecular connectivity or physical properties known about the system (e.g., physical density).

Model NSLD profiles can be also obtained from computer simulations. In molecular dynamics (MD) simulations, the ensemble average structure of a system at equilibrium is readily available, and thus, a direct model of the NSLD ($NSLD_{MD}$) is calculable. This information can be used to generate a reflectivity profile from the simulated trajectory, which can be directly compared to the experimental data or used to build an MD-model-based initial guess for the fitting procedure mentioned above. This is particularly appealing, considering the ever-growing performance of computers and efficiency of MD simulation software, and the availability of coarse-grained (CG) models that allow overcoming length- and time-scale limitations of atomistic MD simulations. Similar approaches have already been applied, for example, to fit neutron reflectivity (NR) data of the $\alpha$-hemolysin ion channel reconstituted in tethered lipid bilayers by generating a model of the contribution of the protein to the NSLD profile from a crystal structure.[5] Another example is the software SIMtoEXP (http://sourceforge.net/projects/simtoexp/),[6] which combines MD data with the analysis of small-angle neutron and X-ray scattering (SANS/SAXS) data.

NeutronRefTools is a plugin for the VMD molecular visualization and analysis software;[7] it allows extraction of the $NSLD_{MD}$ from either all-atom (AA) or CG simulations, as well as the calculation of the neutron reflectivity profile. This can be extended to the corresponding electron density and X-ray reflectivity profiles. The corresponding experimental data can also be loaded and directly compared to the simulations. In addition, NeutronRefTools is able to calculate volume fractions and absolute volumes of the components of the system, providing further structural detail, and a basis for molecular scattering length densities models. The combination of these features and the integration into the VMD software package facilitates direct comparison of data, without the need to transfer or convert datasets between MD and neutron scattering software. Two application examples are presented to illustrate the capabilities of the tool. In test case 1, reflectivity profiles obtained from AA and CG MD simulations are compared with experimental data of a DMPC lipid bilayer


DOI: 10.1021/acs.jctc.5b00635
J. Chem. Theory Comput. 2015, 11, 4875−4884

measured in different solvent contrasts. In addition, the molecular volumes, both volume fraction profiles and absolute values, are computed and compared to previous literature reports. In test case 2, the molecular volumes in pure and binary 1,2-di-palmitoyl-*sn*-glycero-3-phosphocholine/1,2-dihexadecanoyl-*sn*-glycero-3-phosphocholine (DOPC/DPPC) lipid bilayers are obtained from AA simulations. This example illustrates the ability of the approach to obtain molecular insight into more experimentally challenging systems.

## METHODS

The NeutronRefTools plugin computes four properties of a system: (i) the NSLD profile, (ii) the volume fraction ($\Phi$) profile of the components, (iii) absolute molecular volumes, and (iv) the reflectivity profile of the system at an interface that can be defined by the user.

Both the NSLD and volume fraction profiles are one-dimensional properties computed along the direction orthogonal to the surfaces of the layers of the system. As an example, a DMPC lipid bilayer/water system with the membrane aligned to the $x-y$ plane will be considered. The dimension in which the NSLD and volume fractions are measured corresponds to the $z$-axis (see Figure 1A).

Once the direction is defined, the system is discretized in layers ($i = 3, ..., N$) along that direction, and the NSLD is calculated in each volume element according to eq 3:

$$\mathrm{NSLD}_{\mathrm{MOL}_j} = \sum_{k=\mathrm{atom\ types}_{\mathrm{MOL}_j} \in \mathrm{Layer}_i} \frac{n_k b_k}{V_{\mathrm{Layer}_i}} \tag{3}$$

where $n_k$ is the number of atoms of type $k$ corresponding to a given molecular species $\mathrm{MOL}_j$, in a given layer $i$ ($\mathrm{Layer}_i$), $b_k$ is the coherent neutron scattering length for the atom type, and $V_{\mathrm{layer},i}$ is the volume of the layer defined by the $x$ and $y$ dimensions of the box, and the selected bin size in the $z$-direction. The total NSLD value for a given layer is computed via the addition of the NSLD contribution of all molecular species present in the layer.

The volume fraction ($\Phi$) is calculated using eq 4:

$$\Phi_{\mathrm{MOL}_j} = \frac{\sum_{k=\mathrm{atoms}_{\mathrm{MOL}_j} \in \mathrm{Layer}_i} V_k}{V_{\mathrm{Layer}_i}} \tag{4}$$

where $V_k$ is the volume of an atom from a given molecular species $\mathrm{MOL}_j$ located in a given layer ($\mathrm{Layer}_i$). The calculation of each $V_k$ is performed by using a three-dimensional (3D) Voronoi tessellation of the system (NeutronRefTools uses the Voro++ library[8] for this purpose) per layer or for the complete system box, where the former is slower than the latter.

These calculations can be iterated over selected MD trajectory frames, providing average values per layer, which are finally used to generate the $\mathrm{NSLD}_{\mathrm{MD}}(z)$ and $\Phi_{\mathrm{MD}}(z)$ profiles. The $\mathrm{NSLD}_{\mathrm{MD}}(z)$ is the quantity compared to experimentally fitted NSLD profiles, and its decomposition in molecular contributions, as well as that of the $\Phi_{\mathrm{MD}}(z)$, allows interpreting the structure of the system in terms of the spatial distribution of its components. NeutronRefTools allows the user to decompose the $\mathrm{NSLD}_{\mathrm{MD}}(z)$ and $\Phi_{\mathrm{MD}}(z)$ in a very flexible manner by creating as many atomic groups as desired/required.

It is worth emphasizing that the calculation of the $\mathrm{NSLD}_{\mathrm{MD}}$ in the present approach is independent of the volume fraction calculation. As indicated by eq 3, the NSLD is obtained using the volume of each layer ($V_{\mathrm{layer},i}$) in which the system has been discretized.

The calculation of absolute molecular volumes is also based on the construction of three-dimensional (3D) Voronoi cells for each atom of the system. However, in this case, no partition over layers is required and the reported value corresponds to the volume (in units of Å$^3$) of the selected group of atoms (see eq 5) from each frame of the MD trajectory.

$$\mathrm{Vol}_{\mathrm{MOL}_j} = \sum_{k=\mathrm{atoms}_{\mathrm{MOL}_j}} V_k \tag{5}$$

To account for the boundaries of the system in the tessellation process, the dimensions of the box are passed to Voro++ to define the planes to cut the Voronoi cells of those particles close to the box edge for every MD snapshot. This process could incur volume underestimation but will likely be minimized by averaging over MD frames.

A challenging aspect of the present approach in the calculation of volumes is the presence of void space in the simulation box, which induces an overestimation of the volume for those particles surrounding the "hole". This is certainly a limitation to the general applicability of this approach. However, when the void space corresponds to a slab of vacuum, e.g., water/vacuum interface, the overestimation is minimized when the system is suitably partitioned, instead of using the entire box (tessellation per layer mentioned above).

Conversely, 3D Voronoi tessellation provides a consistent measurement of effective molecular volumes that responds to environmental effects and phase changes, while relying only on the position of the particles during the simulation.

Finally, the reflectivity profile is calculated using the Abeles matrix method.[4] This approach is commonly used in the fitting of experimental neutron scattering data, in packages such as MOTOFIT,[9] Reflpak/Refl1D (http://www.ncnr.nist.gov/reflpak/), GenX (http://genx.sourceforge.net), Parratt (http://www.physics.brocku.ca/~tharroun/parratt/), and many others (http://material.fysik.uu.se/Group_members/adrian/reflect.htm#Analysis). Typically, the thickness and NSLD of each layer in a model are parameters optimized during the fitting procedure, starting from an initial guess defined by the user. In NeutronRefTools, this somewhat arbitrary initial guess is replaced by the MD-based structure of the system (Figure 1B), from which the reflectivity profiles for different neutron contrasts can be generated by defining the deuteration level of, e.g., the solvent or other molecular constituents.

To describe the reflectivity calculation, let us consider an incident neutron beam that is refracted by each of the layers considered in Figure 1B. The value of the wavevector $k$ in layer $n$ is given by eq 6:

$$k_n = \sqrt{\left(\frac{Q}{2}\right)^2 - 4\pi(\mathrm{NSLD}_n - \mathrm{NSLD}_0)} \tag{6}$$

where $Q$ is the momentum transfer (see eq 2). From the wavevectors corresponding to two adjacent layers (for example, $n$ and $n + 1$), the Fresnel reflection coefficient between those layers can be calculated using eq 7:

$$r_{n,n+1} = \frac{k_n - k_{n+1}}{k_n + k_{n+1}} \exp(-2k_n k_{n+1} {\sigma_{n,n+1}}^2) \tag{7}$$



DOI: 10.1021/acs.jctc.5b00635
J. Chem. Theory Comput. 2015, 11, 4875−4884

where a Gaussian modification is applied to account for the roughness/diffuseness of each interface, as described by Nevot and Croce.[10] Using the Fresnel coefficient for each interface and a phase factor ($\beta_n$), which accounts for the thickness of each layer (see eq 8), a characteristic matrix ($C_n$) is constructed for each layer $n$, as shown in eq 9.

$$\beta_n = \begin{cases} 0 \leftrightarrow n = 0 \\ k_n \times \text{thickness}_n \leftrightarrow 1 \leq n \leq N \end{cases} \tag{8}$$

$$C_n = \begin{bmatrix} \exp(i\beta_{n1}) & r_n \exp(i\beta_{n1}) \\ r_n \exp(-i\beta_{n1}) & \exp(-i\beta_{n1}) \end{bmatrix} \tag{9}$$

Considering the product of the characteristic matrices for all the layers, a resultant matrix is obtained usingeq 10:

$$\mathbf{M} = \prod_{n=0}^{N} C_n \tag{10}$$

whose elements $M_{11}$ and $M_{21}$ give the reflectivity corresponding to a given $Q$ value (eq 11):

$$R(Q) = \frac{M_{21}M_{21}^*}{M_{11}M_{11}^*} \tag{11}$$

In addition to the graphical comparison between the experimental and theoretical reflectivity profiles, NeutronRefTools also provides a more quantitative comparison by means of the reduced $\chi^2$ metric, calculated as indicated in eq 12:

$$\chi^2 = \frac{\sum_{i=1}^{N_q} \frac{(R_{\text{exp}}(Q) - R_{\text{MD}}(Q))^2}{\text{sd}_{\text{exp}}^2}}{N_q - 1} \tag{12}$$

where $N_q$ refers to the number of $q$ values for which the experimental and MD-based reflectivities ($R_{\text{exp}}(q)$ and $R_{\text{MD}}(q)$, respectively) were measured, and the parameter $\text{sd}_{\text{exp}}$ corresponds to the experimental standard deviation of each data point. The usage of the reduced $\chi^2$ value may be useful in the selection of the parameters during the fitting procedure.

To account for the experimental resolution, that is, the relative error associated with the $Q$ values ($dq/Q$), NeutronRefTools also offers the option to smear the reflectivity profile by means of discrete convolution with Gaussian functions with user-defined fwhm (full width at half maximum) and number of points for discretizing the Gaussian. In the present approach, the Gaussian fwhm equals the absolute error $dq$, obtained from $dq/Q$ for each $Q$ value in the reflectivity profile. The value of $dq/Q$, in turn, can be a user-defined constant, or read directly for each point from the experimental data file.

NeutronRefTools implementation of the methods described above allows the user to choose different computing options and input specific parameters, depending on the desired property to be calculated. In the case of the NSLD and molecular volume calculations, some of the available options are (i) the model type (AA or CG); (ii) the calculation type (NSLD and/or molecular volumes); (iii) trajectory-related options (i.e., range of frames to be analyzed and/or how many are selected (e.g., 1 every 10 frames)); (iv) the thickness of the layers into which the simulation box will be split; (v) the percentage of solvent deuteration; (vi) the selection of atoms for the decomposition of the NSLD and volume fraction profiles, with their respective deuteration; and (vii) the selection of atoms to compute the absolute volumes.

Regarding the reflectivity calculation, the main options include: (i) the $Q$ range to evaluate the reflectivity (input manually or read from the experimental data file); (ii) parameters such as the incoherent *background* noise in the experimental data; (iii) the selection of the $\text{NSLD}_{\text{MD}}$ region to be used, and the parameters of any additional layers, such as substrate material for supported bilayers, to generate an MD-based NSLD of the full system (e.g., the substrate-lipid bilayer-water interface) that represents the experimental setup. For example, to compare a MD simulation of a lipid bilayer in water with a supported bilayer experiment, the $\text{NSLD}_{\text{MD}}$ is used to generate layers 3 to $N$, representing the solvated bilayer and, layers 0, 1, and 2 are used to model the supporting surface (i.e., layer 0, silicon wafer; layer 1, $SiO_2$ surface; and layer 2, optional layer of solvent between the surface and membrane), and layer $N + 1$ is used to complete the system with an infinitely thick layer of bulk water (see Figure 1). In addition, by removing a suitable number of points from the $\text{NSLD}_{\text{MD}}$, the amount of water between the bilayer and the supporting surface can be adjusted to match the experimental system.

In neutron reflectivity experiments, the method of contrast variation allows one to selectively highlight or hide different molecular components of the system by partial or complete deuteration of the components and/or the solvent. Because of the notable difference in the coherent scattering length between hydrogen and deuterium, this approach leads to multiple reflectivity profiles with different intensity for the same physical system. Accordingly, for a given structural model to be considered correct, it must reproduce the reflectivity profiles for all of the experimentally generated contrasts/deuteration schemes.

NeutronRefTools allows the selection of a percentage of the solvent and/or specific components of the system, to be deuterated and the generation of the corresponding NSLD and reflectivity profiles, which can be compared to the corresponding experimental measurements. It is important to bear in mind that this approach is a first approximation based on assuming equivalent dynamics for deuterated and nondeuterated molecules. Alternatively, multiple simulations, each with the desired deuteration level, can be performed and analyzed independently with NeutronRefTools.

**Molecular Models.** The simulation of processes involving surfaces, interfaces, or thin films, such as lipid bilayers, is often computationally expensive because of the large system size and long time-scales required to sample the conformations of interest. For this reason, analysis of MD trajectories generated using CG models, in addition to AA simulations, is available. In particular, the current implementation is compatible with the SDK CG force-field.[11−13] In the current version, there is no special treatment for the CG beads in the generation of the volume fraction profiles. As in the AA case, the Voronoi cell is generated for each particle, weighted by the radius (AA or CG), and the entire volume of the cell is assigned to the layer where the center of the bead is located. This is the reason for the choice of a bin-size of 6 Å in the CG volume fraction profile in test case 1 (see Results). An alternative approach, where the cell volume is split between the layer that contains the center of the particle and the two adjacent layers was also considered. In this case, the proportion of volume assigned to each layer is dependent on the distance of the center of the particle relative to the boundaries of the layer containing it. From such a


DOI: 10.1021/acs.jctc.5b00635
J. Chem. Theory Comput. 2015, 11, 4875−4884

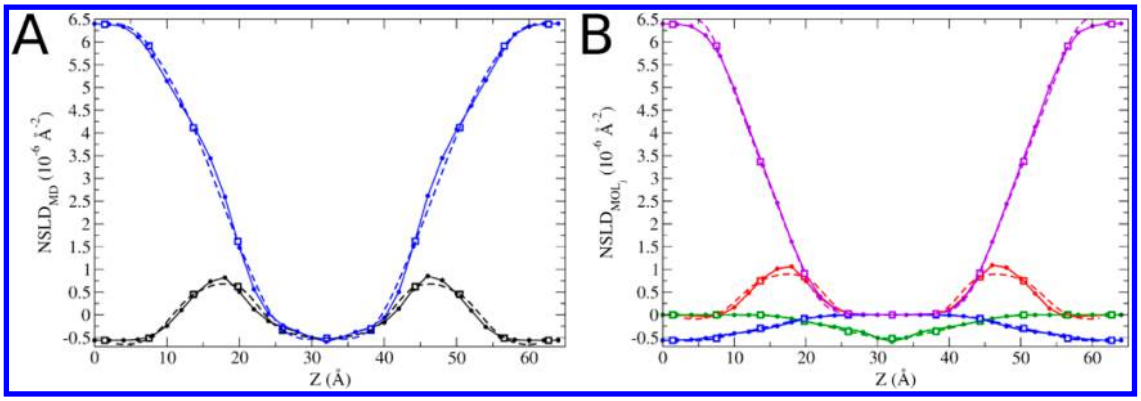


**Figure 2.** NSLD profiles. (A) NSLD profile for a DMPC bilayer in $H_2O$ (black traces) or $D_2O$ (blue traces) from MD-AA (continuous line/filled circles) and MD-CG (empty squares: computed values, dotted lines: interpolation between computed values) simulations, analyzed with NeutronRefTools. (B) Decomposition of the NSLD profile into lipid molecular components (red, head groups; green, lipid tails) and solvent (blue, $H_2O$; violet, $D_2O$) for both MD-AA (continuous line/filled circles) and MD-CG (empty squares: computed values, dotted lines: interpolation between computed values) data.

distance, the fraction of the cell volume corresponding to each layer could be estimated assuming a spherical particle. However, as potential artifacts might arise with such assumption, in addition to a higher computational cost, the previously described simpler approach was preferred.

*Test Case 1. Neutron Reflectivity of a DMPC Bilayer.* The first model example consists of generating the NSLD, volume fraction, and reflectivity profiles for a DMPC lipid bilayer from MD simulations at both atomistic and coarse-grained levels, and comparison with experimental reflectivity data. For this purpose, a pre-equilibrated lipid bilayer containing 120 DMPC (1,2-dimyristoyl-*sn*-glycero-3-phosphocholine) molecules was placed in a rectangular box with the bilayer plane aligned to the $x-y$ plane. The system was solvated using the Solvate plug-in of VMD[7] and water molecules overlapping with the lipids were removed. The CHARMM36[14] force-field was used for the lipids and the TIP3P model[15] for water. Initial steric clashes were removed by 5000 steps of minimization, followed by 500 ps of equilibration with restraints on the phosphate groups to maintain the thickness of the bilayer during the relaxation/thermalization of the system. MD simulations were performed in the NpT ensemble, with a semi-isotropic pressure coupling at 1 atm using the Nose−Hoover Langevin piston,[16] while the temperature was controlled at 303 K by means of the Langevin thermostat.[17] Long-range electrostatic interactions were treated using the particle mesh Ewald algorithm,[18] and van der Waals forces were smoothly switched off, using the vdwForceSwitching option, between 10 Å and 12 Å. The RATTLE algorithm[19] was used to constrain all bonds involving hydrogen atoms, in order to use a time step of 2 fs. The multitime step algorithm r-RESPA[20] was used to integrate the equations of motion. Nonbonded short- and long-range forces were computed every time step. A 120 ns AA simulation was generated using NAMD2.9 (http://www.ks.uiuc.edu/Research/namd/).[21] Subsequently, the all atom system was mapped into the SDK model[13] using in-house Tcl scripts. A CG-MD simulation of 1 $\mu$s was generated using LAMMPS (http://lammps.sandia.gov).[22] The system was evolved in the NpT ensemble using Velocity Verlet time integration with a Nose−Hoover thermostat and barostat,[23] with a semi-isotropic pressure coupling at 1 atm, and the temperature controlled at 303 K. A cutoff of 15 Å for nonbonded interactions was used in combination with long-range electrostatic interactions evaluated using the PPPM method.[24] A time step of 10 fs was used to integrate the equations of motion.

For the experimental counterpart, specular neutron reflection of a supported bilayer of DMPC on a 80 mm × 50 mm × 15 mm silicon (111) wafer was measured in $H_2O$ and $D_2O$ on the D17 reflectometer[25] at the Institut Laue Langevin (Grenoble), using neutron wavelengths $\lambda$ of 2−20 Å and two angles of incidence (0.7° and 3.0°). The supported bilayer was formed by *in situ* vesicle fusion (0.5 mg/mL DMPC SUV in $D_2O$, formed by tip sonication) after measuring the silicon substrate reflectivity in $D_2O$ and $H_2O$. Initial optical matrix modeling of the structure was performed using three layers (head groups, tails, head groups) to describe the lipid bilayer, which was found to have a total thickness of 41 ± 2 Å, with an average area per molecule of 62 ± 5 Å$^2$, and a polar head-group thickness of 7 ± 1 Å. The support surface had a $SiO_2$ layer with a thickness of 12 ± 2 Å, 24 v/v% solvent and interfacial roughness of 2.5 Å (toward the Si) and 2.5 Å (toward the solution).

*Test Case 2. Calculation of Molecular Volumes for DOPC and DPPC Lipids in One- and Two-Component Bilayers at Two Different Temperatures.* The second application considered is the calculation of lipid volume changes with varying temperature and composition from AA simulations of single and mixed DOPC and DPPC bilayers. To this extent, two lipid bilayers containing 108 DOPC (1,2-dioleoyl-*sn*-glycero-3-phosphocholine) and 116 DPPC (1,2-di-palmitoyl-*sn*-glycero-3-phosphocholine) molecules were placed in two rectangular boxes with the bilayer plane aligned to the $x-y$ plane. In addition, a mixed DOPC/DPPC bilayer was built using 56 DOPC and 56 DPPC molecules, placed in a rectangular box and aligned to the $x-y$ plane. The three systems were solvated and equilibration and production runs were performed using the same methods and parameters as those used in the AA simulations of test case 1. Two temperature values were considered (298 and 323 K). The centers of mass of the phosphate groups in the DPPC bilayer simulation at 298 K were subjected to a sequence of restraints with force constants of 1, 0.1, 0.01, and 0.001 kcal/mol for 8 ns in the first instance and 4 ns in each of the subsequent restraints, respectively, in order to keep the interleaflet distance separation at 43 Å, and to achieve an equilibrated bilayer in the gel phase. Such equilibration was followed by 50 ns of production MD.


DOI: 10.1021/acs.jctc.5b00635
J. Chem. Theory Comput. 2015, 11, 4875−4884

**Table 1. Parameters Used in the Reflectivity Calculations**[a]

| | | | | | Solvent (% v/v) | |
|---|---|---|---|---|---|---|
| layer | composition | NSLD ($\times 10^{-6}$ Å$^{-2}$) | thickness (Å) | roughness (Å) | MD | $MD_{corr}$ |
| 0 | Si | 2.07 | | | 0.0 | 0.0 |
| 1 | $SiO_2$ | 3.41 | 12.0 | 2.5 | 24 | 24 |
| 2 | $H_2O/D_2O$ | −0.56/6.36 | 0.0 | 0.0 | 0.0 | 0.0 |
| 3, ..., $N$ | MD average | $NSLD_{MD}$ | 2.0[b] \| 6.0[c] | 0.0 | 40[d] \| 0[e] \| 40[f] | 10[d] \| 15[e] \| 35[f] |
| $N$ + 1 | $H_2O/D_2O$ | −0.56/6.36 | | 2.5 | 100 | 100 |

[a]Background values of $2 \times 10^{-7}$ and $2 \times 10^{-6}$ were used for $H_2O$ and $D_2O$, respectively. The first 10 Å of $NSLD_{MD}$ were removed, to mimic the supported bilayer setup. [b]AA simulation. [c]CG simulation. [d]Maximum solvent volume fraction at the head groups next to the supporting surface. [e]Maximum solvent volume fraction at the lipid tails. [f]Maximum solvent volume fraction at the head groups far from the supporting surface.

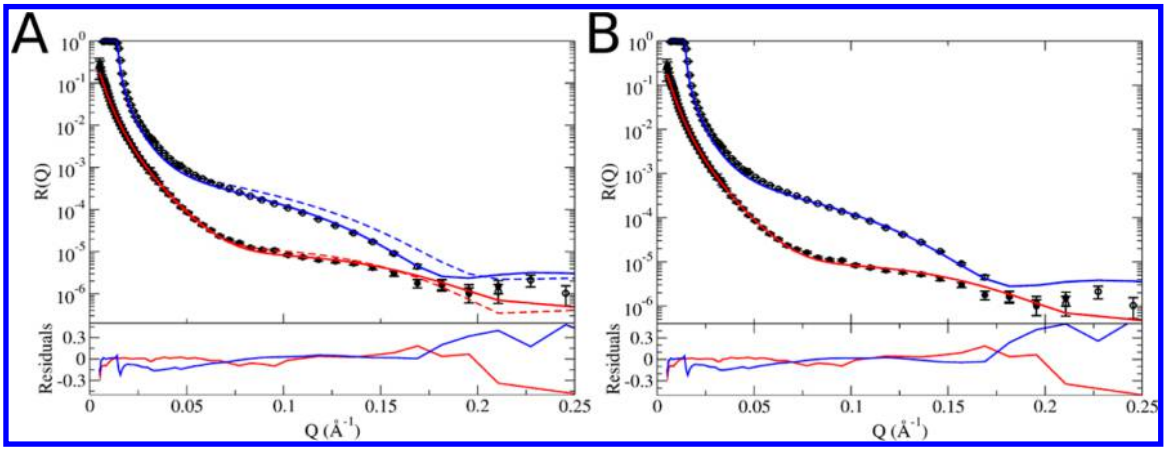


**Figure 3.** Reflectivity profiles. (A) Experimental reflectivity data for a DMPC lipid bilayer in $H_2O$ and $D_2O$ (filled and empty black circles, respectively), considering a constant resolution smearing (d$q$/$Q$) of 0.1, is compared to the theoretical data obtained from AA-MD trajectories, based on the $NSLD_{MD}$ profiles in $H_2O$ (red traces) and $D_2O$ (blue traces), with (continuous lines) and without (dotted lines) the water content correction at the head-groups and tails regions (see Table 1 for further detail). The residuals, calculated as the difference between the logarithm of the reflectivity from the MD and the logarithm of the experimental reflectivity, is shown in the bottom plot for $H_2O$ and $D_2O$ (red and blue traces, respectively). (B) Same as that for panel A, but using the $NSLD_{MD}$ profiles from CG-MD trajectories, with the water content correction.

Equilibrated patches of liquid-phase DOPC and gel-phase DPPC bilayers were used to generate the mixed DOPC/DPPC system for the simulation at 298 K. This configuration was further equilibrated for 20 ns, and a production run of 50 ns was used for analysis. The area per lipid was calculated using MEMBPLUGIN.[26]

## RESULTS

**Test Case 1. Neutron Reflectivity of a DMPC Bilayer.** NeutronRefTools was used to calculate the NSLD, reflectivity, and volume fraction profiles from AA and CG MD trajectories of a DMPC bilayer/water system. The MD-based reflectivity data was compared with experimental measurements for a supported DMPC bilayer in water and deuterated water. In addition, the molecular volumes were also calculated and compared to experimental values reported in the literature. Comparison of the total $NSLD_{MD}$ profiles calculated for both AA and CG MD trajectories for the DMPC bilayer (Figure 2A), and their decomposition into molecular component contributions (Figure 2B) illustrates the potential of the tool in the analysis of both molecular representations. Moreover, in this example, a good agreement between AA and CG simulations is also achieved. As mentioned earlier, the generation of multiple contrasts is required to attain a reliable structural model to interpret the experimental reflectivity data. Figure 2A shows the $NSLD_{MD}$ for the DMPC bilayer system in both 100% of the $H_2O$ and after replacement of all solvent molecules by $D_2O$. The degree of substitution can be chosen by the user by specifying the percentage of water molecules to randomly substitute by deuterated water. Combining the computed $NSLD_{MD}$ with the definition of parameters for the substrate/solvent layers 0, 1, 2 and $N$ + 1, and the instrument background (see the Methods section, and Table 1), the reflectivity profiles for the DMPC bilayer system were computed in water and deuterated water. One consideration at this point is that the $NSLD_{MD}$ obtained from simulations of a lipid bilayer using periodic boundary conditions by definition corresponds to a solvent volume fraction at the lipid tails level of zero (except in the presence of water pores). In contrast, in supported bilayer experiments, the supporting surface is usually not perfectly covered by the lipids but patches of water can remain in membrane defects affecting the reflectivity profile and the corresponding effective NSLD of the bilayer. This situation can be addressed by correcting the $NSLD_{MD}$ to include a variable level of solvent volume fraction at the lipid tails level, until a good fit between MD and experimental reflectivity is obtained. An initial guess to the amount of water at the lipid tails can be estimated from the difference in MD and experimental area per lipid, when the latter corresponds to the area occupied by both solvent and lipids. In the present example, the experimental area per lipid is 62 ± 5 Å$^2$, while the values measured from the MD trajectories are 61 ± 2 Å$^2$ for AA and 60 ± 1 Å$^2$ for CG. This indicates that the initial guess would be on the order of the experimental relative error in the area per lipid (~9%).


DOI: 10.1021/acs.jctc.5b00635
J. Chem. Theory Comput. 2015, 11, 4875−4884

Consistent with the previous consideration, the raw reflectivity profiles generated from the AA MD trajectories (Figure 3A) indicate a disagreement between the experimental and MD data (dotted traces), particularly clear in the $D_2O$ contrast. Besides the water content at the lipid tails region, an alternative (or complementary) explanation for this inconsistency could also be a difference in the water content at the head-group level. This could be a consequence of the contact between the bilayer and the supporting solid surface in the experiment, while such an interaction is absent in the MD simulation. To test this hypothesis, the $NSLD_{MD}$ and associated reflectivity profiles were tuned to consider variations in the solvent volume fraction at the head-groups and lipid tails levels (see Table 1). Using this approach, a corrected MD-based reflectivity profile, showing a reasonable fit to the experimental data, was obtained (Figure 3A, continuous traces). This result indicates that the water content in supported and free bilayers differ at the head-group level, supporting the previous hypothesis. However, it also suggests that the MD data of a free bilayer in solution can, in fact, be used for the fitting of supported bilayer neutron reflectivity data, as long as the water content at the head-groups and lipid tails levels is properly considered. The suitability of this approach is also evidenced when comparing the water content corrected reflectivity profiles obtained from CG-MD simulations with the experimental data (Figure 3B).

Although reasonable good fits have been obtained using the present approach, some residual disagreement between experimental and MD reflectivity profiles still remains. Besides the aforementioned differences in the lipid bilayer water content, another source of error could reside in the absence of an explicit supporting surface in the molecular simulations. In other words, mixing free bilayer molecular simulations data with artificial layers representing the supporting material might fail to mimic subtle structural constraints induced on the lipids by the surface, which would translate into small differences in the NSLD and reflectivity profiles. However, the present approach has the advantage of being independent from the availability/development of suitable force field representations of the supporting surface materials.

Finally, the results obtained for both AA and CG models not only illustrate the applicability of the method but also highlight its potential use in testing different molecular representations and force fields for molecular simulations. In addition, the results point to a distinct difference in the head-group hydration in free and solid-supported bilayers. It has long been debated whether the solid support imposes constraints on the molecular conformation, mobility, or dynamics of the lipids, albeit without conclusive evidence.

The volume fraction calculation using NeutronRefTools relies exclusively on the position and radii of the particles. From this data, the radical Voronoi tessellation of Voro++[8] is used to construct the Voronoi cell around each atom or CG bead in the system, and obtain the associated particle volume for each simulation frame. Such per particle data is then gathered by molecular component, defined by the user, and plotted along the $z$-axis. Figure 4 shows the output corresponding to the DMPC/water system for both AA and CG MD data. While the calculation for the AA system was done using layers 2 Å thick, the higher granularity of the CG model required layer thicknesses of 6 Å to accommodate the bulkier beads. Consequently, in general, fewer data points are generated in the CG volume fraction profiles. For this reason, intermediate

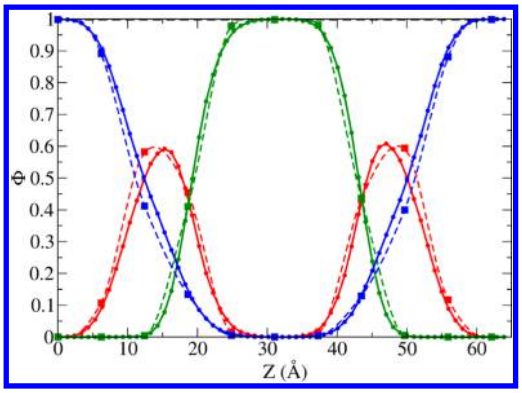


**Figure 4.** Volume fraction profiles for a DMPC bilayer in $H_2O$, decomposed in lipid molecular components (red, head groups; green, lipid tails) and water (blue) contributions, generated from MD-AA (continuous line/filled circles) or MD-CG (filled squared represent computed values, dotted lines represent interpolation between computed values) simulations, using NeutronRefTools.

data points were interpolated between the CG measurements to facilitate graphical comparison. Despite the different level of detail between the AA and CG representations, generally good agreement is observed, particularly in the regions containing pure water ($z < 7$ Å, $z > 57$ Å) or pure lipids (15 Å $< z <$ 45 Å). Unsurprisingly, slight differences are observed at the lipid/water interface, because of the granularity of the CG water model (one CG water is composed of three all-atom water molecules). These data can be complemented by the calculation of the molecular volumes to obtain the absolute volume for any component of the system. As shown in Table 2,

**Table 2. Molecular Volumes for a DMPC Bilayer/$H_2O$ System[a]**

| | Volume (Å$^3$) | | |
|---|---|---|---|
| molecular component | MD-AA | MD-CG | Exp |
| head group | 403.0 ± 2.0 | 411.0 ± 1.0 | |
| lipid tails | 713.0 ± 4.0 | 690.0 ± 1.0 | |
| lipid | 1115.0 ± 4.0 | 1101.0 ± 1.0 | 1101 (from ref 31) |
| water | 28.9 ± 0.4 | 84.3[b] ± 0.4 | 30.3 (from ref 27) |

[a]Calculated executing Voro++[8] from NeutronRefTools. [b]3 × 28.1 = 84.3.

the calculated volumes for the DMPC lipids are in good agreement with previously reported values. In particular, the CG model renders a surprisingly accurate value, while the AA model slightly overestimates the average lipid volume. When the latter is decomposed in head-group and lipid-tail contributions, the overestimation observed in the AA model can be attributed to a higher volume of the lipid tails. Note the slightly higher volume of the CG head groups, which is consistent with the volume fraction difference at the lipid/water interface mentioned earlier. Finally, water volumes for both the AA and CG models are in good agreement with previous reports.[27] It should be mentioned that the calculation of molecular volumes from molecular simulations can be used to compute the SLD values for a given molecular species in a specific environment. Such volume data are well characterized for certain systems, such as, for example, phosphatidylcholine bilayers, but for other types of lipids, mixtures, or new


DOI: 10.1021/acs.jctc.5b00635
J. Chem. Theory Comput. 2015, 11, 4875−4884

materials, such information might not be available, turning molecular simulations into a very valuable source.

**Test Case 2. Calculation of Molecular Volumes for DOPC and DPPC Lipids in One- and Two-Component Bilayers at Two Different Temperatures.** Lipid mixtures are a good example where molecular simulations could contribute valuable information not accessible easily experimentally by providing an estimation of the change in molecular volumes in different environments and at different phases. To illustrate this, the volumes of DOPC and DPPC lipids in one and two-component bilayers, at 298 and 323 K were obtained from analyzing atomistic simulations using NeutronRefTools. Figure 5 shows the distribution of lipid volumes during the simulations, and Table 3 summarizes the average values. To complement to volumetric data, the area per lipid was also calculated for each system and is reported in Table 3. Agreement between the calculated volumes and areas from the MD simulations and those from previous experimental reports[28−30] is found for both DOPC and DPPC lipids in one-component liquid-phase bilayers (Table 3). The lipid-dependent influence of temperature is evidenced by a considerable decrease in the DPPC volume (~90 Å$^3$), as a consequence of the liquid-gel phase transition, compared to a small decrease (~26 Å$^3$) in the DOPC volume, because of the heat removal from the system, without phase transition. A similar trend is observed when considering lipid mixtures, although the extent of the volume changes is reduced as a consequence of the coexistence of a DPPC bilayer domain in the gel phase with a DOPC bilayer domain in the liquid phase (Figure 6). To rationalize the data, the lipid mixture at 323 K (both lipids in the liquid phase) will be considered first and subsequently, the effect of reducing the temperature to 298 K. At 323 K, the average volume of a DOPC lipid in the one-component bilayer is equal to the corresponding volume in the two-component system, within statistical error. The same observation stands for the DPPC lipid, as shown in Figure 5 and Table 3. Therefore, the differences found in the volume change when comparing the one-component systems and mixtures are not a consequence of the behavior of the bilayer when both lipids are in the liquid phase. Hence, the difference must occur at 298 K where, in fact, slightly higher values in both DOPC (~14 Å$^3$) and DPPC (~31 Å$^3$) lipid volumes are observed in the mixture, compared to the one-component systems. In the case of the DPPC, an important contribution comes from DPPC molecules at the boundaries of the gel-phase domain that lose tail order when they are in contact with DOPC molecules in the liquid-phase (see Figures 5 and 6A). This is evidenced when considering the lipid volumes of the DPPC molecules not in contact with DOPC molecules, as shown in Figure 5 (gray trace). In that case, the sampled molecular volumes are more similar to the one-component bilayer distribution. In the DOPC case, the slightly higher volume that is observed seems to be more evenly distributed among DOPC molecules, because no shift in the volume distribution was observed for molecules that were not in contact with DPPC lipids. Finally, to take this analysis one step further, the lipid volumes were decomposed in head-group and lipid-tail contributions (see Table 4). For both lipid species, the lipid tails are the main contributors to the increased volume values in the two-component system at 298 K, which account for 100% of the change in the DOPC volume and 74% in the case of the DPPC lipid. In summary, the coexistence of liquid and gel phase domains in a lipid bilayer induces an increase in the volume of both components, mainly localized in the lipid tails, and more marked in the gel-phase lipids, which reside at the boundary between lipid domains.

The lipid-dependent influence of temperature is also evidenced when considering the area per lipid (apl) in the one-component systems. In fact, while no effect is observed for

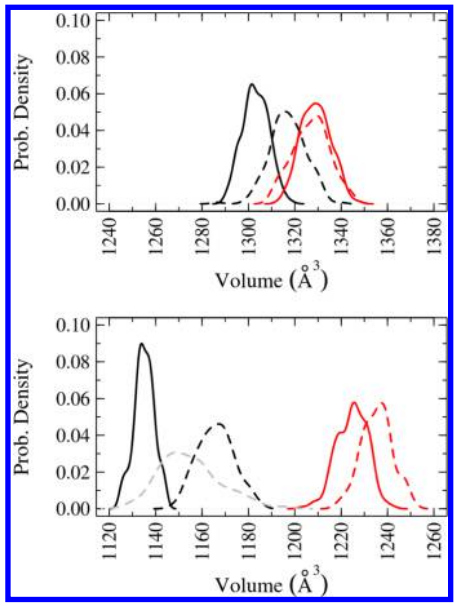


**Figure 5.** Distribution of molecular volumes for DOPC/DPPC mixtures at 298 and 323 K. The average volume distribution for DOPC (top) calculated for single (continuous line) DOPC and mixed (dotted line) DOPC/DPPC bilayer at 298 K (black traces) and 323 K (red traces) is shown. The corresponding distributions for DPPC are shown in the bottom panel. The gray dotted trace corresponds to DPPC molecules not in contact with DOPC molecules in the mixed system at 298 K.

**Table 3. Volume per Lipid (vpl) and Area per Lipid (apl) for DOPC and DPPC in One- and Two-Component Bilayers**[a]

| | One-Component Bilayer | | | | Two-Component Bilayer | | | |
|---|---|---|---|---|---|---|---|---|
| | DOPC | | DPPC | | DOPC | | DPPC | |
| temp (K) | vpl[b] (Å$^3$) | apl (Å$^2$) | vpl[b] (Å$^3$) | apl (Å$^2$) | vpl[b] (Å$^3$) | apl (Å$^2$) | vpl[b] (Å$^3$) | apl (Å$^2$) |
| 298 | 1303 ± 6<br>*1303* (from ref 28) | 67 ± 1<br>*67.4* (from ref 30) | 1135 ± 4 | 49 ± 1 | 1317 ± 8 | 64 ± 2 | 1166 ± 8 | 51 ± 1 |
| 323 | 1329 ± 9 | 69 ± 1 | 1225 ± 7<br>*1232* (from ref 28) | 59 ± 2<br>*63.1* (from ref 29) | 1327 ± 8 | 65 ± 2 | 1235 ± 7 | 65 ± 2 |

[a]Experimental values are indicated in italics. [b]Molecular volumes were calculated executing Voro++[8] from NeutronRefTools.



DOI: 10.1021/acs.jctc.5b00635
J. Chem. Theory Comput. 2015, 11, 4875−4884

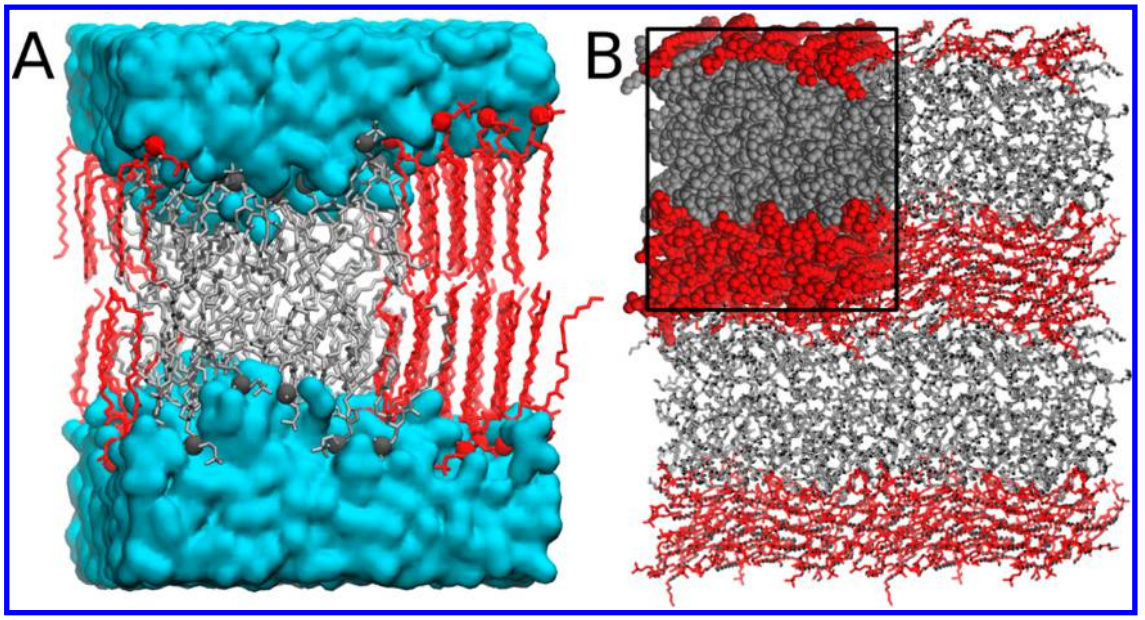


**Figure 6.** DOPC/DPPC mixture at 298 K. (A) Lateral view of the simulated system showing phase separation between DPPC lipids in the gel-phase and DOPC lipids in the liquid-phase (red and gray licorice representation, respectively). The aqueous environment is represented as a cyan surface. (B) Top view of the simulated system cell (gray and red van der Waals (vdW) representations corresponding to DOPC and DPPC lipids, respectively) surrounded by three periodic boundary condition replicas. Gray and red licorice representations correspond to DOPC and DPPC lipids, respectively.

**Table 4. Molecular Volume Decomposition at 298 K Calculated by Executing voro++[8] from NeutronRefTools**

| | Lipid Volume (Å$^3$) | | | |
|---|---|---|---|---|
| | DOPC | | DPPC | |
| lipid constituent | one-component | mixture (DOPC + DPPC) | one-component | mixture (DOPC + DPPC) |
| head group | 399 ± 2 | 401 ± 3 | 388 ± 2 | 396 ± 3 |
| lipid tails | 904 ± 5 | 916 ± 7 | 747 ± 4 | 770 ± 7 |

DOPC, a reduction of ∼10 ± 2 Å$^2$ is registered in the apl of DPPC, as a consequence of the phase transition. The same trend is also observed in the two-component systems, where no change in the apl of DOPC is associated with the change in temperature, while the area of the DPPC lipids is reduced by ∼14 ± 2 Å$^2$. This is consistent with the DPPC head groups conserving the gel phase structure, as confirmed by the indistinguishable (within statistical error) area per lipid values at 298 K in both one- and two-component systems. Unlike the behavior of the volume per molecule, attenuation of the change in apl is not observed when reducing the temperature. This indicates that the reduced effect of the temperature on the lipid volumes observed in the two-component system, as compared to the one-component system, must be localized in the lipid tails instead of the head groups. This is consistent with the behavior of the molecular volumes mentioned earlier, and with a molecular picture where the lipid tails appear to be more sensitive than the head groups, with regard to the presence of another lipid type in a different phase.

## ■ CONCLUSIONS

A novel tool for the analysis of reflectivity data from macromolecular systems and lipid bilayers using MD simulations is presented in this manuscript. The tool is implemented as a VMD plug-in, adding the possibility to extract neutron-scattering-related properties from atomistic and coarse-grained MD trajectories to the MD analysis toolbox already available in the VMD software. The main observables retrieved by NeutronRefTools are the reflectivity profile and the accompanying neutron scattering length density. This allows for a direct comparison between MD data and raw experimental information. In addition, the volume fraction and absolute molecular volumes can be calculated to gain atomic/molecular detail about the structure of the system under study, which is particularly useful for mixtures, new materials, or complex systems where these values are not known from previous experimental studies. The tool comes with a graphical interface to facilitate data input. In particular, the choice to select atomic contributions to measured properties is available. The software aims to promote the use of MD simulations in the neutron scattering community, as well as facilitating the use of neutron scattering data as a source for model validation/construction by the simulation community. Extension of the implemented procedures could be made to also calculate X-ray reflectivity, using the electron density instead of the nuclear distribution and NSLD, contributing to the integration of both experimental approaches with MD simulations.

Two practical applications have been considered: (1) the calculation of the neutron reflectivity of a DMPC bilayer, and (2) the calculation of molecular volumes for DOPC and DPPC lipids in one- and two-component bilayers at two different temperatures, showing the advantages and limitations of the presented tool.

Finally, NeutronRefTools is expected to collaborate with existing open-source programs for scattering calculations (e.g., Motofit, SASView, or SimToExp) to facilitate data analysis.



DOI: 10.1021/acs.jctc.5b00635
J. Chem. Theory Comput. 2015, 11, 4875−4884

Such interoperability will allow scientists to seamlessly use different levels of physical description. Ultimately, scientists planning experiments on neutron facilities could refine their design and interpretation using knowledge based on computation.

## AUTHOR INFORMATION


### Corresponding Authors

*E-mail: hanna.wacklin@esss.se (H. Wacklin).
*E-mail: carmen.domene@kcl.ac.uk (C. Domene).


### Notes

The authors declare no competing financial interest.

## ACKNOWLEDGMENTS

We would like to acknowledge the use of computational resources from the EPSRC UK National Service for Computational Chemistry Software (NSCCS), the Hartree Center, and Temple University via a National Science Foundation Major Research Instrumentation Grant (No. CNS-09-58854). This work was supported by the Biotechnology and Biological Sciences Research Council.

## REFERENCES


(1) Hardt, S. L. Rates of Diffusion Controlled Reactions in One, Two and Three Dimensions. *Biophys. Chem.* **1979**, *10*, 239−243.

(2) Penfold, J.; Richardson, R. M.; Zarbakhsh, A.; Webster, J. R. P.; Bucknall, D. G.; Rennie, A. R.; Jones, R. A. L.; Cosgrove, T.; Thomas, R. K.; Higgins, J. S.; Fletcher, P. D. I.; Dickinson, E.; Roser, S. J.; McLure, I. A.; Hillman, A. R.; Richards, R. W.; Staples, E. J.; Burgess, A. N.; Simister, E. A.; White, J. W. Recent Advances in the Study of Chemical Surfaces and Interfaces by Specular Neutron Reflection. *J. Chem. Soc., Faraday Trans.* **1997**, *93*, 3899−3917.

(3) Higgins, J. S.; Benoît, H. *Polymers and Neutron Scattering*; Oxford Series on Neutron Scattering in Condensed Matter; Clarendon Press: Oxford, U.K., 1994.

(4) Heavens, O. S. *Optical Properties of Thin Solid Films*; Butterworths Scientific Publications: London, U.K., 1955.

(5) McGillivray, D. J.; Valincius, G.; Heinrich, F.; Robertson, J. W. F.; Vanderah, D. J.; Febo-Ayala, W.; Ignatjev, I.; Losche, M.; Kasianowicz, J. J. Structure of Functional *Staphylococcus aureus* Alpha-Hemolysin Channels in Tethered Bilayer Lipid Membranes. *Biophys. J.* **2009**, *96*, 1547−1553.

(6) Kucerka, N.; Katsaras, J.; Nagle, J. F. Comparing Membrane Simulations to Scattering Experiments: Introducing the Simtoexp Software. *J. Membr. Biol.* **2010**, *235*, 43−50.

(7) Humphrey, W.; Dalke, A.; Schulten, K. VMD: Visual Molecular Dynamics. *J. Mol. Graphics* **1996**, *14*, 33−38.

(8) Rycroft, C. H. Voro++: A Three-Dimensional Voronoi Cell Library in C++. *Chaos* **2009**, *19*, 041111.

(9) Nelson, A. Co-Refinement of Multiple-Contrast Neutron/X-ray Reflectivity Data Using Motofit. *J. Appl. Crystallogr.* **2006**, *39*, 273−276.

(10) Nevot, L.; Croce, P. Characterization of Surfaces by Grazing X-ray Reflection—Application to Study of Polishing of Some Silicate-Glasses. *Rev. Phys. Appl.* **1980**, *15*, 761−779.

(11) Shinoda, W.; DeVane, R.; Klein, M. L. Coarse-Grained Molecular Modeling of Non-Ionic Surfactant Self-Assembly. *Soft Matter* **2008**, *4*, 2454−2462.

(12) Shinoda, W.; DeVane, R.; Klein, M. L. Zwitterionic Lipid Assemblies: Molecular Dynamics Studies of Monolayers, Bilayers, and Vesicles Using a New Coarse Grain Force Field. *J. Phys. Chem. B* **2010**, *114*, 6836−6849.

(13) Shinoda, W.; DeVane, R.; Klein, M. L. Coarse-Grained Force Field for Ionic Surfactants. *Soft Matter* **2011**, *7*, 6178−6186.

(14) Klauda, J. B.; Venable, R. M.; Freites, J. A.; O'Connor, J. W.; Tobias, D. J.; Mondragon-Ramirez, C.; Vorobyov, I.; MacKerell, A. D., Jr.; Pastor, R. W. Update of the Charmm All-Atom Additive Force Field for Lipids: Validation on Six Lipid Types. *J. Phys. Chem. B* **2010**, *114*, 7830−7843.

(15) Jorgensen, W. L.; Chandrasekhar, J.; Madura, J. D.; Impey, R. W.; Klein, M. L. Comparison of Simple Potential Functions for Simulating Liquid Water. *J. Chem. Phys.* **1983**, *79*, 926−935.

(16) Martyna, G. J.; Tobias, D. J.; Klein, M. L. Constant-Pressure Molecular-Dynamics Algorithms. *J. Chem. Phys.* **1994**, *101*, 4177−4189.

(17) Izaguirre, J. A.; Catarello, D. P.; Wozniak, J. M.; Skeel, R. D. Langevin Stabilization of Molecular Dynamics. *J. Chem. Phys.* **2001**, *114*, 2090−2098.

(18) Essmann, U.; Perera, L.; Berkowitz, M. L.; Darden, T.; Lee, H.; Pedersen, L. G. A Smooth Particle Mesh Ewald Method. *J. Chem. Phys.* **1995**, *103*, 8577−8593.

(19) Andersen, H. C. Rattle—A Velocity Version of the Shake Algorithm for Molecular-Dynamics Calculations. *J. Comput. Phys.* **1983**, *52*, 24−34.

(20) Tuckerman, M.; Berne, B. J.; Martyna, G. J. Reversible Multiple Time-Scale Molecular-Dynamics—Reply. *J. Chem. Phys.* **1993**, *99*, 2278−2279.

(21) Phillips, J. C.; Braun, R.; Wang, W.; Gumbart, J.; Tajkhorshid, E.; Villa, E.; Chipot, C.; Skeel, R. D.; Kale, L.; Schulten, K. Scalable Molecular Dynamics with NAMD. *J. Comput. Chem.* **2005**, *26*, 1781−1802.

(22) Plimpton, S. Fast Parallel Algorithms for Short-Range Molecular-Dynamics. *J. Comput. Phys.* **1995**, *117*, 1−19.

(23) Hoover, W. G. Constant-Pressure Equations of Motion. *Phys. Rev. A* **1986**, *34*, 2499−2500.

(24) Frenkel, D.; Smit, B. *Understanding Molecular Simulation: From Algorithms to Applications*, Second Edition; Computational Science Series; Academic Press: San Diego, CA, 2001.

(25) Cubitt, R.; Fragneto, G. D17: The New Reflectometer at the ILL. *Appl. Phys. A: Mater. Sci. Process.* **2002**, *74*, S329−S331.

(26) Guixa-Gonzalez, R.; Rodriguez-Espigares, I.; Ramirez-Anguita, J. M.; Carrio-Gaspar, P.; Martinez-Seara, H.; Giorgino, T.; Selent, J. MEMBPLUGIN: Studying Membrane Complexity in VMD. *Bioinformatics* **2014**, *30*, 1478−1480.

(27) Petrache, H. I.; Feller, S. E.; Nagle, J. F. Determination of Component Volumes of Lipid Bilayers from Simulations. *Biophys. J.* **1997**, *72*, 2237−2242.

(28) Nagle, J. F.; Tristram-Nagle, S. Structure of Lipid Bilayers. *Biochim. Biophys. Acta, Rev. Biomembr.* **2000**, *1469*, 159−195.

(29) Kucerka, N.; Nieh, M. P.; Katsaras, J. Fluid Phase Lipid Areas and Bilayer Thicknesses of Commonly Used Phosphatidylcholines as a Function of Temperature. *Biochim. Biophys. Acta, Biomembr.* **2011**, *1808*, 2761−2771.

(30) Kucerka, N.; Nagle, J. F.; Sachs, J. N.; Feller, S. E.; Pencer, J.; Jackson, A.; Katsaras, J. Lipid Bilayer Structure Determined by the Simultaneous Analysis of Neutron and X-ray Scattering Data. *Biophys. J.* **2008**, *95*, 2356−2367.

(31) Kucerka, N.; Liu, Y. F.; Chu, N. J.; Petrache, H. I.; Tristram-Nagle, S. T.; Nagle, J. F. Structure of Fully Hydrated Fluid Phase DMPC and DLPC Lipid Bilayers Using X-ray Scattering from Oriented Multilamellar Arrays and from Unilamellar Vesicles. *Biophys. J.* **2005**, *88*, 2626−2637.




DOI: 10.1021/acs.jctc.5b00635
*J. Chem. Theory Comput.* 2015, 11, 4875−4884